



Analysis of Surface Strain Distribution over the Biaxial Stretch-Formed and Deep-Drawn Cups of Cu-Cr-Zr-Ti Alloy Thin Sheet

Dibya Ranjan Behera, Sushanta Kumar Panda,
Sujoy Kumar Kar, K. Thomas Tharian and
S.V.S. Narayana Murty

EasyChair preprints are intended for rapid
dissemination of research results and are
integrated with the rest of EasyChair.

May 12, 2023

Analysis of surface strain distribution over the biaxial stretch-formed and deep-drawn cups of Cu-Cr-Zr-Ti alloy thin sheet

1st Dibya Ranjan Behera
Department of Mechanical Engineering
IIT Kharagpur
Kharagpur-721302, India
ranjan123dibya@gmail.com

4th K. Thomas Tharian
Liquid Propulsion Systems Centre
Valiamala, ISRO
Thiruvananthapuram-695547, India
k_thomastharian@lpsc.gov.in

2nd Sushanta Kumar Panda
Department of Mechanical Engineering
IIT Kharagpur
Kharagpur-721302, India
sushanta.panda@mech.iitkgp.ac.in

5th S.V.S. Narayana Murty
Liquid Propulsion Systems Centre
Valiamala, ISRO
Thiruvananthapuram-695547, India
narayanamurty_susarla@lpsc.gov.in

3rd Sujoy Kumar Kar
Department of Metallurgical and
Materials Engineering
IIT Kharagpur
Kharagpur-721302, India
sujoy.kar@metal.iitkgp.ac.in

Abstract— In the present study, the strain distribution profiles were determined by deforming the Cu-Cr-Zr-Ti alloy sheets through stretch forming and deep drawing experiments, and the limiting dome height (LDH) and cup depth of the deformed components were evaluated. The finite element (FE) models of both the processes were developed by incorporating the Hill48 anisotropy yield criterion and Hollomon power hardening law to predict the strain distribution profiles. The LDH of the stretch-formed component was 20 mm, whereas the cup depth obtained from the deep drawing process was 33.5 mm. In stretch forming experiment, the strain localization was observed at a distance of 17.14 mm from the pole with major and minor strain values of 0.43 and 0.19, respectively. The top edge of the deep-drawn cup wall region was found to deform under radial tension-circumferential compression mode, whereas the deformation at the cup corner region followed close to plane strain mode with major and minor strain values of 0.12 and 0.04, respectively. Also, the grain size, precipitates and texture were characterized through optical microscopy, SEM-EDS and EBSD techniques. This material showed excellent formability without orange peel and earing defects in the deformed samples due to its higher n -value of 0.46, lower grain size of 25-30 μm and negligible planar anisotropy parameter of -0.04.

Keywords—Cu-Cr-Zr-Ti alloy, Microstructure, Stretch forming, Deep drawing, FE modeling, Strain distribution

I. INTRODUCTION

Copper (Cu) and its alloys can be used in various heat transfer components such as inner shell of thrust chamber and nozzle liner in satellite launch vehicles [1-2]. However, the application of pure Cu for different thermo-structural components is limited due to its lower strength at higher working temperatures within the range of 500–600 °C. In this regard, various alloying elements such as chromium (Cr), zirconium (Zr), titanium (Ti) etc. are added in order to enhance the strength through the formation of Cr-rich precipitates. The solubility of Cr is found to be only about 0.37 wt.% in Cu matrix, occurring at 1077 °C. This imposes a constraint in improvement of strength by solid solution strengthening of Cr [3]. The further improvement in the

strength and ductility at higher temperature can be achieved by minor addition of Zr and Ti. The addition of Zr helps in the formation of fine Cr precipitates and uniformly distributes them in the alloy thereby providing resistance to the softening behavior at the required working temperature. Moreover, the presence of Ti in the alloy prevents the sulphur embrittlement and coarsening of precipitates [4]. Therefore, Cu-Cr-Zr-Ti alloy can be a potential material for the fabrication of inner liners of regeneratively cooled cryogenic and semi cryogenic engines of satellite launch vehicles in view of its improved strength at higher temperature, higher thermal conductivity, enhanced ductility, resistance to fatigue and creep failure due to addition of the alloying elements[5].

The thrust chamber liners used in cryogenic engines contain convergent and divergent sections, which can be fabricated through multistage forming processes such as deep drawing and subsequent redrawing. It is noteworthy that during the multistage forming process, the material is subjected to different modes of deformation at different locations. Hence, it becomes important to understand the ability to deform successfully during these deformation modes. This ability of the material to deform successfully without strain localization and failure is termed as formability of the sheet material. The forming behavior depends upon the material properties, which include the mechanical and metallurgical properties of the materials, the process parameters such as the blank holding force (BHF), coefficient of friction, stress state of the material and the strain bounding criteria, which include the failure modes and surface roughness. The successful fabrication of components therefore depends upon the careful selection of the above parameters.

The formability of the sheet metal is generally evaluated in terms of LDH, limiting drawing ratio (LDR) and strain distribution profile depending upon the mode of deformation. The LDH is the method of evaluating the formability in case of stretch forming process, whereas the LDR is commonly used during the deep drawing process

[6]. The strain distribution profile developed on the deformed components, and becomes an important formability measure for determining the quality of the formed components. This profile indicates the mode of deformation and uniformity in strain distribution, which can affect the depth and thinning development in the deformed component. It also depicts the location of failure and helps as a diagnostic tool in understanding the deformation behavior during the forming process.

In this context, the main objectives of the present research identified as given below.

- (i) To evaluate the formability related mechanical properties of the novel Cu-Cr-Zr-Ti alloy sheet material, and to study the microstructure and micro texture.
- (ii) To conduct the stretch forming and deep drawing tests of the above alloy, and to experimentally evaluate the surface strain distributions of the deformed components.

Also, FE modelling of the these processes were developed using anisotropic and strain hardening properties of the material, and the predicted strain distributions were validated with the experimental results.

II. MATERIALS AND METHODS

A. Microstructural Characterizations

In the present work, as received hot rolled Cu-Cr-Zr-Ti alloy sheets were considered having a composition (wt. %) of 0.5% Cr, 0.05% Zr, 0.05% Ti and remaining Cu. This alloy was further solutionized at 950 °C for 30 min and subsequently water quenched to dissolve the strengthening precipitates (Cr) into the matrix and to get uniform grain structure. The oxide scales present on the surface of the sheets were removed using a solution containing the mixture of HCl and deionized water of equal weight %. The samples for microstructure characterization were prepared as per the standard procedure mentioned elsewhere [7], and the prepared surface was etched with a solution of $K_2Cr_2O_7$ (2 gm), H_2SO_4 (8 ml) and H_2O (100 ml). The microstructure of of this alloy was examined under the optical microscope. The precipitates were characterized through scanning electron microscope (SEM). The EBSD scan was carried out with a step size of 1 μm to analyze the texture through inverse pole figure (IPF). In this regard, the specimen was prepared by electro-polishing method using an electrolyte containing HPO_3 (25 ml), C_2H_5OH (25 ml) and deionized H_2O (50 ml) at 6 V for 20 sec. These scans were analyzed through TSL software to obtain the IPF map.

B. Tensile Test

The uniaxial tensile test of the solutionized sheet was conducted in order to evaluate the important mechanical properties such as the yield strength (YS), ultimate tensile strength (UTS), % total elongation, strength coefficient (K - value) and strain hardening exponent (n -value). In this regard, standard sub-sized specimens with 30 mm gauge length were cut from the sheet, and these were further deformed at a crosshead speed of 2 mm/min. The

Funding for this research was received from ISRO (details in acknowledgement).

engineering stress (S) vs strain (e) and true stress ($\bar{\sigma}$) vs strain ($\bar{\epsilon}$) curves were obtained from load-displacement data. The material parameters, both the K -value and n -value, were determined from the true stress-strain curve using the Hollomon hardening law, $\bar{\sigma} = K\bar{\epsilon}^n$. The plastic anisotropy (r -value), signifying the resistance of the material to thinning, were evaluated along rolling (r_0), transverse (r_{90}), and diagonal (r_{45}) directions with reference to rolling direction of the sheets using Eq. (1). In this regard, the specimens were deformed to a displacement corresponding to 80% of UTS [8], and both the width and longitudinal strains were measured after the deformation. The normal anisotropy (\bar{r}) and planar anisotropy (Δr) of this material were estimated using Eq. (2) and Eq. (3).

$$r\text{-value} = \frac{\epsilon_w}{\epsilon_t} = \frac{\epsilon_w}{-(\epsilon_1 + \epsilon_w)} \quad (1)$$

Where ϵ_1 , ϵ_w and ϵ_t are longitudinal strain, width strain and thickness strain, respectively.

$$\bar{r} = \frac{1}{4}(r_0 + 2r_{45} + r_{90}) \quad (2)$$

$$\Delta r = \frac{1}{2}(r_0 - 2r_{45} + r_{90}) \quad (3)$$

C. Forming Test

The laboratory-scale experimental test setup for both the stretch forming and deep drawing processes consisting of the dies, binders and punches were designed and fabricated using D2 steel. The dimensions of all the components along with the schematic view of both the test setups is shown in Fig. 1. Both the deformation processes were performed in a 100-ton double action hydraulic press. In case of the stretch forming process, a sub-sized hemispherical punch of ϕ 45 mm was used, whereas a flat bottom cylindrical punch of ϕ 50 mm was used for the deformation in the deep drawing process. A square sample with dimensions of 100×100 mm² was used to achieve biaxial deformation mode in the stretch forming process, whereas circular blank of ϕ 95 mm was deformed in the deep drawing process. The blank, in case of both the deformation processes, was clamped in between the die and binder with the application of BHF of 95 kN and 7.5 kN during the stretch forming and deep drawing process, respectively. The punch was allowed to move down and deform the blank in both the cases. In deep drawing experiment, a sufficient amount of grease was applied on both sides of blank for lubrication and easy flow of material, whereas, the stretch forming experiment was conducted in dry condition. The deformation in case of the stretch forming process was stopped at the onset of necking. However, the deep drawing process was performed by moving the punch in downward, and it was found that the load initially increased with advancement of the punch, reached a peak value and subsequently decreased to zero indicating that the blank was completely drawn into the die cavity. Prior to the beginning of both the experimental processes, the blanks were electrochemically etched with

circular grids of ϕ 2.5 mm. The shape of the circular grids changed to ellipse after deformation and hence, the principal strains i.e., the major strain and minor strain generated during both the deformation processes were evaluated from the corresponding major and minor diameters of the ellipse with reference to the original grid diameter using the circular grid analysis given in Eq. 4.

$$\varepsilon_1 = \ln\left(\frac{d_1}{d_0}\right), \varepsilon_2 = \ln\left(\frac{d_2}{d_0}\right) \quad (4)$$

Where, d_1 = major diameter of the ellipse, d_2 = minor diameter of the ellipse, and d_0 = initial circular grid diameter

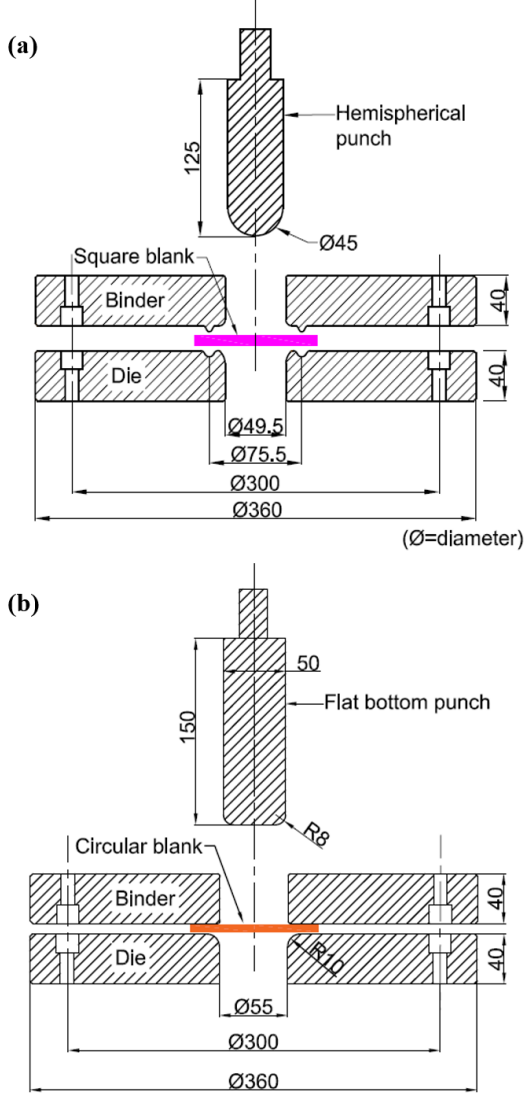


Fig. 1. Schematic of (a) stretch forming test setup and (b) deep drawing test set up used in the present study (all dimensions are in mm)

III. FE MODELING

The FE modelling of both the stretch forming and deep drawing processes were carried out in the LS-dyna software (LS-971 version). The die, binder and punch were modelled as rigid bodies, and the dimensions of these tools were

maintained same as those provided in the experimental setup. The die was assigned as a stationary tool, whereas the punch was imparted with a velocity of 1000 mm/s. A draw bead was created at ϕ 75.5 mm on binder in order to restrict the flow of material during stretch forming process. The blank was modeled as Belytschko-Tsay shell elements with 1 mm mesh size. The blank was modelled using the Hill48 anisotropy yield criterion represented by *MAT-122 material card in the software. Also, the strain hardening behavior was incorporated into the material model. The Hill48 yield criterion can be mathematically expressed as Eq. 6 for plane stress deformation mode. The friction during the deformation process was assumed to follow Coulomb's law, and the coefficient of friction during the stretch forming and the deep drawing process was assigned as 0.2 and 0.1, respectively. The FE modelling was performed in order to predict the deformation behavior in terms of strain distribution, location of strain localization and cup depth.

$$\sigma_{Hill} = \bar{\sigma} = \sqrt{\sigma_1^2 - \frac{2r_0}{1+r_0}\sigma_1\sigma_2 + \frac{r_0(1+r_{90})}{r_{90}(1+r_0)}\sigma_2^2} \quad (6)$$

IV. RESULTS AND DISCUSSION

A. Microstructure

The optical and SEM microstructures of solution-treated Cu-Cr-Zr-Ti alloy sheet are shown in Fig. 2. The optical micrograph of this alloy reveals typical equiaxed grain structure along with large number of annealing twins. The average grain size was found \sim 25-30 μ m. The SEM micrograph showed the presence of precipitates whose composition was characterized by EDS point analysis. The Fig. 2(c) shows prominent peaks of Cr along with Cu, confirming these precipitates to be Cr-rich. The solubility of Cr is negligible at room temperature. Hence, as-solutionized and quenched material (Cu-Cr-Zr-Ti) remained in highly super-saturated condition, and a few Cr-rich precipitates were observed [9-10]. These precipitates were found to be in various shapes like spherical, triangular and needle shape. Further, the IPF map was generated using EBSD for the solution-treated specimen and is shown in Fig. 2(d). The map illustrates the orientation of grains and twins with respect the normal direction of sample.

The orange peel defect in the deformed component can be eliminated by selecting sheet materials of finer grain size. It was reported in previous literature that the grain size of material should be less than 80 μ m in order to avoid this orange peel defect [11]. In the present work, after the adoption of the solution heat treatment procedure, the grain size of the material was found \sim 25-30 μ m. This grain size was found to be suitable for the large deformation, and no orange peel defect was observed during the forming experiments. In addition, these finer grains have large grain boundary, which can accommodate more embrittlement phases and hence, can act as barrier for crack propagation during the deformation process [12].

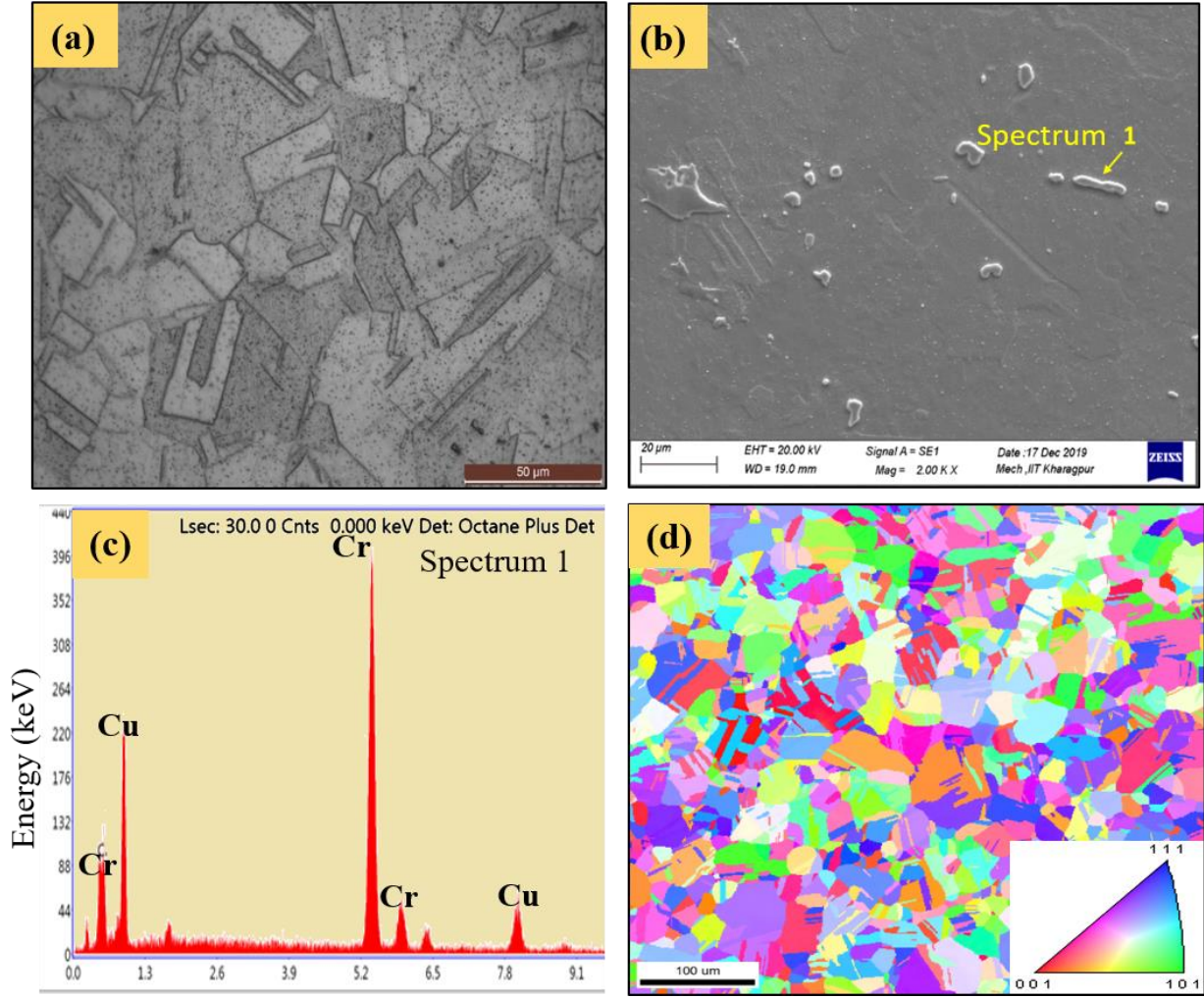


Fig. 2. (a) Optical micrograph with annealed twins, (b) SEM image showing Cr-rich precipitates, (c) EDS spectrum of Cr precipitate and (d) IPF map of Cu-Cr-Zr-Ti alloy

B. Mechanical Properties

The mechanical properties of Cu-Cr-Zr-Ti alloy sheet material were evaluated, and are given in Table 1. The Fig. 3(a) depicts the engineering and true stress-strain curve of this alloy. The true stress-strain curve was obtained using the equations, $\sigma = S(1 + e)$ and $\epsilon = \ln(1 + e)$. This material possessed a YS and UTS of 60 MPa and 204 MPa, respectively. The % total elongation was found to be approximately 46%, out of which the uniform and post uniform elongation were 43% and 3%, respectively. The data in the plastic range of the true stress-strain curve were curve fitted as shown in Fig. 3(b) using a linear regression equation, and the n and K values were estimated. It was observed that the material possessed a very high n -value and uniform elongation suitable for the fabrication of convergent divergent section of the thrust chamber through sheet metal forming process routes. Also, the anisotropic ratios r_0 , r_{45} and r_{90} were found to be 0.69, 0.66 and 0.62, respectively. The normal and planar anisotropy parameters of this alloy were to be 0.66 and -0.04, respectively. Hence, the material showed lower resistance to thinning and higher resistance to earing defects.

TABLE 1: Mechanical properties of solution treated Cu-Cr-Zr-Ti alloy sheet

YS (MPa)	UTS (MPa)	% total elongation	n -value	K -value (MPa)	\bar{r}	Δr
60	204	46	0.46	464.3	0.66	-0.04

C. Surface Strain Distribution and FE Validation

The deformed component after the stretch forming experiment is shown in Fig. 4(a). As the material possessed a very high n -value and excellent ductility, the failure was observed in the form of visible necking in the sample without any sudden fracture, and hence, the experiment could be stopped at the visible of necking. The LDH, defined as the maximum height of the dome or the deformed component at the onset of necking, was found to be 20 mm. The Fig. 4(b) depicts the FE predicted result of the blank stretch formed up to the experimental dome height. The FE simulations captured the maximum strain localization zone (in terms of % thinning) of the deformed sample similar to that of the experimental result. In case of the deep drawing process, a cup of maximum height of 33.5 mm was successfully drawn from the 95 mm diameter blank as shown in Fig. 5(a). It was observed that the drawn cup was devoid of any earing defects which can be attributed to the

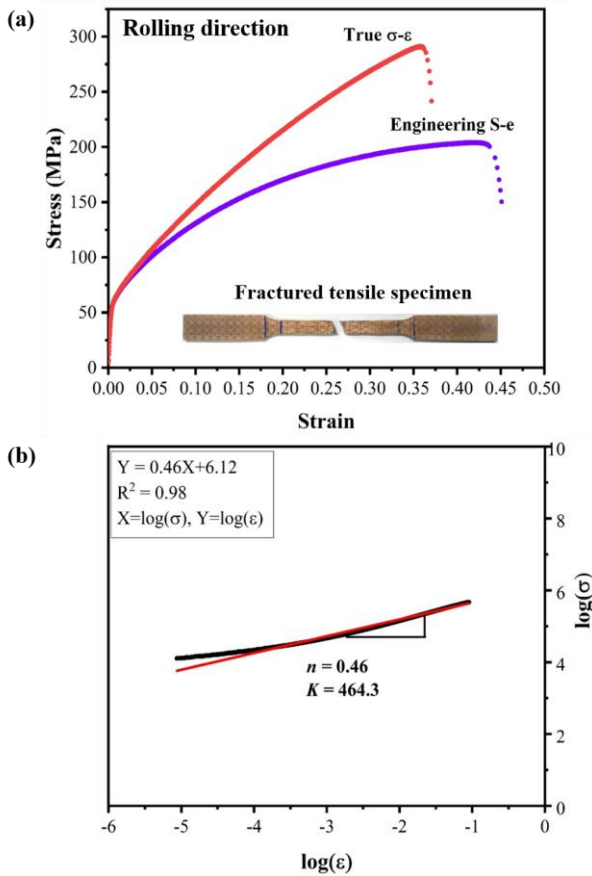


Fig. 3. (a) Engineering and true stress-strain response with fracture tensile specimen and (b) $\log\sigma$ vs. $\log\epsilon$ plot of Cu-Cr-Zr-Ti alloy material

lower value of the planar anisotropic parameter, and this was also well predicted from the FE simulation (Fig. 5(b)). The error in prediction of the deep-drawn cup depth was found to be within 5%.

The surface strains developed on the stretch-formed dome were measured, and plotted against the curvilinear distance from the pole in order to get the strain distribution profile. The pole is defined as the highest point of the deformed dome. The strain distribution profile of the stretch formed dome is shown in Fig. 6(a). It can be noticed from the figure that both the major and minor strains were positive which depicted that the sample underwent biaxial tensile deformation mode. The peak major and minor strain values were found to be 0.43 and 0.19, respectively. These peak values corresponded to the strain localization (necking) region of the deformed component, and this necking location was found to be 17.14 mm from the pole. The strain ratio estimated as the ratio of the minor strain to major strain was found to be approximately 0.44 sufficing the biaxial tensile deformation mode. The FE simulations also predicted a similar strain profile, and the predicted major and minor strains were found to be 0.44 and 0.21, respectively. The location of the strain localization region was predicted at a distance of 16.14 mm from the pole.

In case of the deep drawing process, the surface strains were also evaluated and plotted against the curvilinear distance from the cup center. The obtained strain profile is shown in Fig. 6(b), and it has been divided into three sections, namely cup bottom, cup corner and cup wall. It can be observed that the cup bottom region was subjected to minimal amount of deformation and hence, both the surface

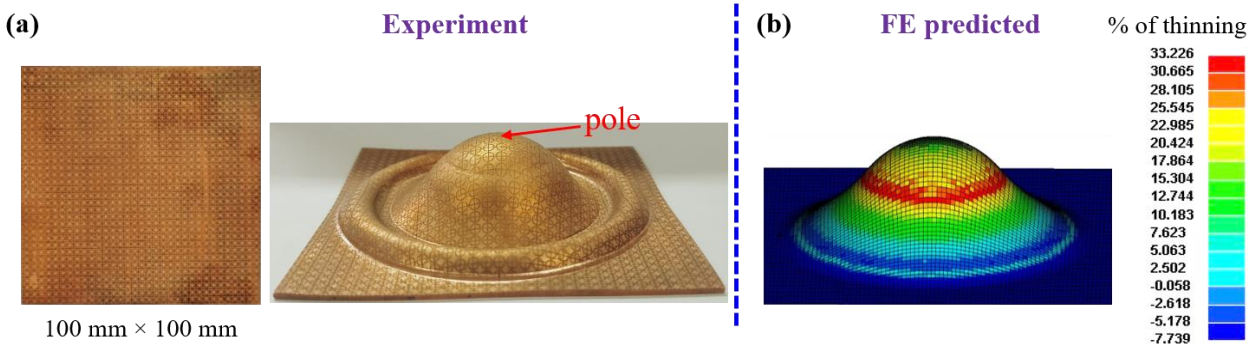


Fig. 4. (a) Experimental bi-axial stretch-formed dome along with the initial blank and (b) FE predicted dome with % of thinning

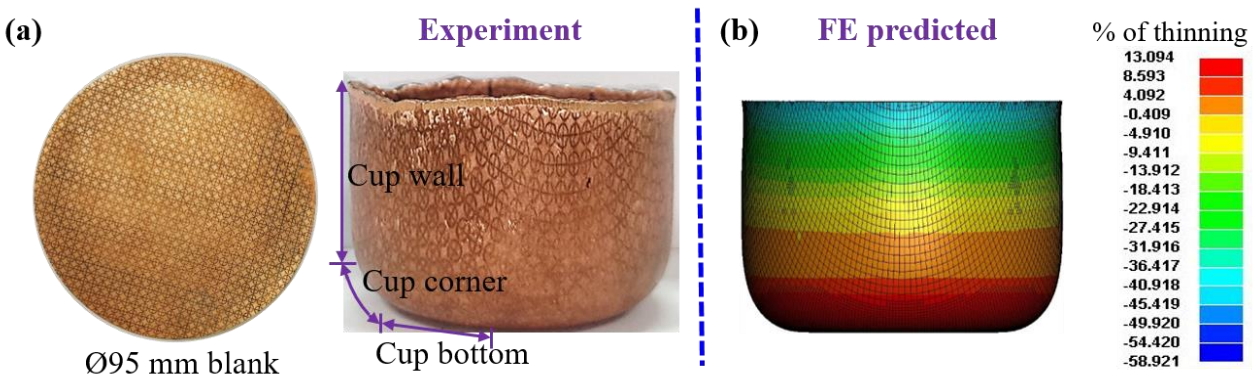


Fig. 5. (a) Experimentally deep-drawn cup along with initial circular blank and (b) FE predicted cup with % of thinning

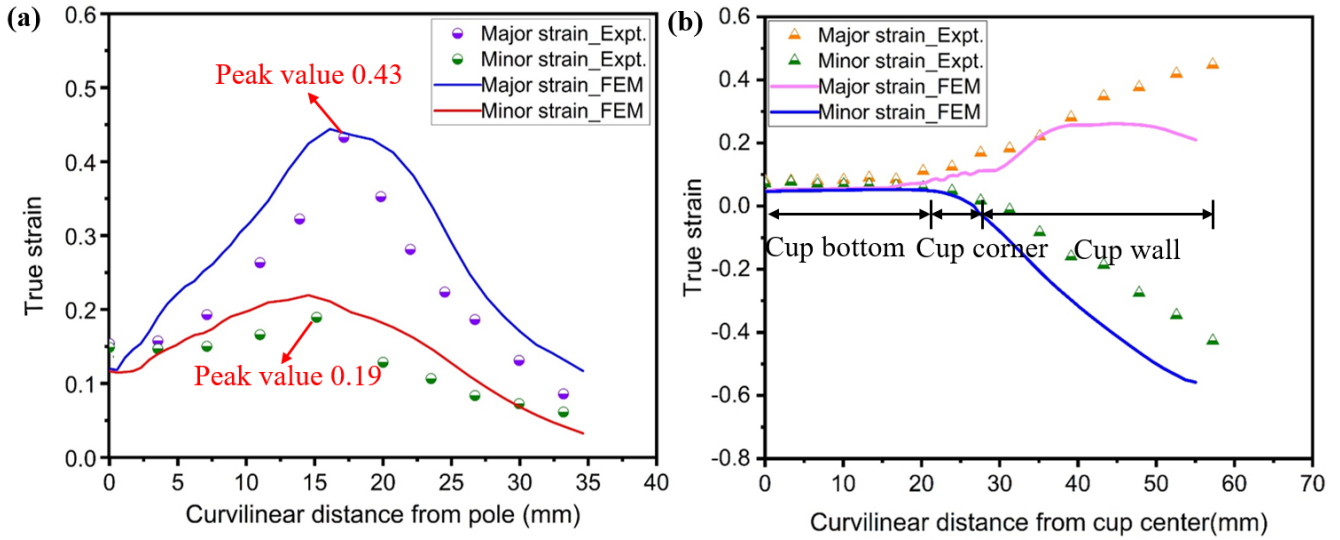


Fig. 6. Experimental and FE predicted surface strain distribution of (a) stretch-formed sample and (b) deep-drawn cup

strain values were negligible. At the cup corner region, the major and minor strain values were found to be approximately 0.12 and 0.04, respectively, which indicated that the deformation was under close to plane strain mode. The higher amount of deformation took place in the cup wall region as can be seen in the Fig. 6(b). The peak strain during the deep drawing process was observed at the top edge of cup, and the values of the peak major and minor strain were 0.45 and -0.42, respectively. These strain values indicated that the material was subjected to a combination of both radial tensile and circumferential compressive deformation mode while drawing into the die cavity. A similar strain distribution profile was also predicted from the FE simulations, and the maximum error in prediction of the strain values was 12%.

The stretch forming process was performed in the dry condition, and the free flow of the material from the flange region into the die cavity was restricted by the application of draw bead and higher BHF of 95 kN. Moreover, frictional force was generated at the punch and sheet interface which was acting radially towards the pole. This force retarded the flow of the material over the punch surface. Hence, the strain localization and significant thinning took place at a distance of 17.14 mm from the pole, and this location lied closer towards the unsupported region leading to failure on further deformation. However, in case of the deep drawing process, the application of BHF was comparatively lower of 7.5 kN and lubrication was applied at the sheet-die and sheet-binder interfaces. This was adopted to facilitate the flow of the material from the flange region into the die cavity during the deep drawing test without the onset of any defects such as flange wrinkling and/or tearing/ necking at the cup corner. The radial tensile strain was induced at cup wall region as the punch forced the sheet material to flow into the die cavity against the frictional resistance at the sheet-tool interface. Simultaneously, the circumference of the blank moved towards the die cavity due to flow of the flange material inducing circumferential compressive strain. Hence, thickening was observed at the top edge of the deformed cup.

V. CONCLUSIONS

The present work dealt with the determination of the mechanical and microstructural properties related to formability of the Cu-Cr-Zr-Ti alloy for fabrication inner liners of cryogenic and semi cryogenic engines of satellite launch vehicle. Also, the forming behavior of this material was investigated in terms of strain distribution, LDH and deformed cup depth through biaxial stretch forming and deep drawing tests. The major conclusions are outlined below.

1. The microstructure of the material depicted typical equiaxed grain structure along with large number of annealed twins. The average grain size was found ~ 25 - $30 \mu\text{m}$ due to which the orange peel defect was not observed in the stretch formed and deep drawn components. Also, Cr-rich precipitates were identified in this alloy under the solutionized condition through SEM-EDS analysis.
2. The YS, UTS, and % total elongation of this alloy sheet were found to be 60 MPa, 204 MPa and 46%, respectively. The material showed an excellent stretchability and deep drawability with LDH of 20 mm and cup height of 33.5 mm, respectively. Also, negligible earing defects were observed in the deep drawn cup which was due to the lower value of planar anisotropy parameter.
3. The surface strain distribution profile of the stretch formed dome was experimentally evaluated. It was observed that both the major and minor strain values were positive with a strain ratio of 0.44 indicating biaxial tensile mode of deformation. The strain localization and significant thinning took place at a distance of 17.14 mm from the pole, and this location lied closer towards the unsupported region.
4. In case of deep drawing, the material at the top edge of cup wall region was observed to deform under radial tension-circumferential compression mode. However, the major and minor surface strains at the cup corner region were found to be 0.12 and 0.04, respectively,

indicating close to plane strain deformation mode. The FE model successfully predicted the surface strain distribution profile, cup depth and location of the strain localization during both stretch forming and deep drawing of Cu-Cr-Zr-Ti alloy sheet material.

ACKNOWLEDGMENT

The authors are greatly thankful to Indian Space Research Organization (ISRO), through Kalpana Chawla Space Technology Cell, IIT Kharagpur (Sanction number-IIT/KCSTC/CHAIR./NEW/P/19-20/01) for financial support.

REFERENCES

- [1] H. Fuxiang et al., "Analysis of phases in a Cu-Cr-Zr alloy," *Scr. Mater.*, vol. 48, no. 1, pp. 97–102, 2003.
- [2] J. Liu et al., "In-situ TEM study of the dynamic interactions between dislocations and precipitates in a Cu-Cr-Zr alloy," *J. Alloys Compd.*, vol. 765, pp. 560–568, 2018.
- [3] S. C. Krishna, G. S. Rao, A. K. Jha, B. Pant, and P. V. Venkitakrishnan, "Strengthening in high strength Cu-Cr-Zr-Ti alloy plates produced by hot rolling," *Mater. Sci. Eng. A-structural Mater. Prop. Microstruct. Process.*, vol. 674, pp. 164–170, 2016.
- [4] K. Saravanan, V. M. J. Sharma, A. K. Asraff, P. Ramesh Narayanan, S. C. Sharma, and K. M. George, "Studies on Dynamic Elastic and Internal Friction Properties of Cu-Cr-Zr-Ti Alloy Between 25 and 650 °C," *J. Mater. Eng. Perform.*, vol. 24, no. 12, pp. 4721–4727, 2015.
- [5] S. V. Narayana Murty, S. Manwatkar, M. George, and P. Ramesh Narayanan, "Microstructural Analysis of a Failed Cu-Cr-Ti-Zr Thrust Chamber Liner of a Cryogenic Engine," *Mater. Perform. Charact.*, vol. 5, no. 5, pp. 648–663, Dec. 2016.
- [6] D. J. Meuleman, J. L. Siles, & J. J. Zoldak, (1985). "The Limiting Dome Height Test for Assessing the Formability of Sheet Steel," *SAE Transactions*, 94, 22–30.
- [7] ASTM E3-11, Standard Guide for Preparation of Metallographic Specimens, ASTM International, West Conshohocken, PA, 2017.
- [8] ASTM E517-19, Standard Test Method for Plastic Strain Ratio for Sheet Metal, ASTM International, West Conshohocken, PA, 2019.
- [9] A. Chbihi, X. Sauvage, and D. Blavette, "Atomic Scale Investigation of Cr Precipitation in Copper," *Acta Mater.*, 2012, 60(11), p 4575–4585.
- [10] M. Kanno, "Effect of Small Addition of Zirconium on Hot Ductility of Cu-Cr Alloy," *Z. Metallkde.*, 1988, 79, p 684–688.
- [11] ASM Metal Hand Book, Forming and Forging, Vol. 14, ASM International, Materials Park, Ohio, (1996), pp.1784-1790, 1933-1942.
- [12] S. C. Krishna, K. V. Radhika, K. T. Tharian, G. S. Rao, M. S. Kiranmayee and B. Pant, "Effect of simulated brazing cycle on the microstructure and mechanical properties of Cu-Cr-Zr-Ti alloy," *Mater. Sci. Forum* Vol.710 (2012) pp. 626-631.